JOURNAL OF COMPUTATIONAL PHYSICS 39, 282–304 (1981)

Finite-Element Method for Time-Dependent Incompressible Free Surface Flow

C. S. FREDERIKSEN AND A. M. WATTS

Department of Mathematics, Queensland University, St. Lucia, 4067, Queensland, Australia

Received October 29, 1979; revised April 2, 1980

We present a finite-element method for time-dependent incompressible free surface fluid flow problems described by the Navier–Stokes equations. The elements chosen have dimensions in both space and time, and the resulting system of equations is block-tridiagonal and lends itself to solution by standard techniques. In the present article we restrict our attention to two-dimensional problems although three-dimensional problems may be solved by a straightforward generalization. The method is essentially an implicit time stepping technique and therefore stable even for relatively large time steps. With this choice of elements, the method is completely adaptive to the changing nature of the solution. An iterative procedure is used to find the position of the free surface; this procedure is found to be rapidly convergent determining accurately the shape of the free surface within a few iterations. Numerical results are given for the problem of entrainment of fluid by a vertically moving plate, which has applications to the chemical engineering problems of the free coating of metals. We also consider the problem of circulation flow in a rectangular channel.

I. INTRODUCTION

The numerical solution of the Navier–Stokes equations for problems with a free boundary is complicated by the need to trace accurately the path in time of the free surface. Problems of this type have been solved by a number of authors (see, e.g. [1–4]) by using finite-difference techniques incorporating a system of marker particles whose movements, when recorded, determine the position of the free surface, or by using a finite-difference approximation of the Lagrangian form of the Navier–Stokes equations, or by using a combination of the above two. While a number of variations of these techniques have been used to solve a wide variety of problems, methods using marker particles have the disadvantage of requiring considerable storage. Recently, finite-element methods have been used for slowly changing and time-independent free surface flow problems [5, 6]; when formulated in this way, the free surface problem takes a very elegant and concise form with the natural boundary condition incorporated within the equations in a straightforward manner.

Jamet and Bonnerot [7–9] have considered one-dimensional problems and recently the two-dimensional Stefan problem using space-time finite elements. In the present

0021-9991/81/020282-23$02.00/0

article we consider flows described by the more complicated two-dimensional Navier–Stokes equations, although there is in principle no difficulty in applying the method to the fully three-dimensional equations. The elements we use have dimensions in both space and time, and, with the appropriate choice of solution vector, the resulting system of equations is block-tridiagonal.

One problem considered in this paper is the entrainment of fluid, by a vertically moving plate, from a bath of fluid of finite depth and the consequent formation of a thin film of fluid on this plate. Such problems concerning the free coating of plates are of interest to chemical engineers [10, 11] and solutions to these problems have generally involved making assumptions about the nature of the flow in various regions of the fluid and then solving the steady-state equations to determine the thickness of the film. We have considered the initial value problem and have traced the formation of the film on the plate by solving the complete Navier–Stokes equation using the finite-element method to be considered below. There exist documented experimental results for this problem ([10] or [11]) and our solutions are in good agreement with these and also the results from the approximate steady-state equations.

The other problem considered in this paper is that of circulation flow in a rectangular channel for which there exists a steady-state solution.

Results for both these problems are presented in Section V.

II. Galerkin Form of Conservation Equations

In Cartesian components the conservation laws for time-dependent incompressible fluid flow may be written as

$$\frac{\partial u_i}{\partial t} + u_j \frac{\partial u_i}{\partial x_j} = f_i + \frac{\partial}{\partial x_j} \sigma_{ij}, \tag{2.1}$$

$$\frac{\partial u_j}{\partial x_j} = 0, \tag{2.2}$$

where u_i is the velocity component in the direction of x_i, f_i the body force component, and σ_{ij} the stress component. For Newtonian flow the following constitutive equation applies,

$$\sigma_{ij} = -p\delta_{ij} + \nu \left[\frac{\partial u_i}{\partial x_j} + \frac{\partial u_j}{\partial x_i} \right], \tag{2.3}$$

where p is the pressure and ν is the kinematic viscosity of the fluid.

If we use (2.2) and (2.3), then (2.1) may be rewritten as

$$\frac{\partial u_i}{\partial t} + \frac{\partial}{\partial x_j} \left(u_j u_i + p\delta_{ij} - \nu \frac{\partial u_i}{\partial x_j} \right) = f_i. \tag{2.4}$$

Conditions on the velocity and stress at a material boundary provide boundary conditions for these equations. Continuity of normal and tangential velocities is applied at a fluid solid interface and continuity of stress with the appropriate allowance for surface tension at a fluid-fluid interface, that is, at a free surface. For the case of a liquid-gas interface, to be considered here, the last condition can be expressed as

$$\sigma_{ij} n_j = \gamma \left(\frac{1}{R_1} + \frac{1}{R_2} \right) n_i, \tag{2.5}$$

where R_1 and R_2 are the radii of curvature of the interface in any two orthogonal planes containing the outward normal $\mathbf{n}$ with components n_i, and γ is the coefficient of surface tension. The authors have found that a finite-element approximation of (2.2) and (2.4) using space-time elements in the manner of Bonnerot and Jamet [7–9] allows for the easy determination of the position of the free surface and also incorporates the natural boundary conditions in a straightforward manner (see below).

Furthermore, because the space domain is continually changing shape, i.e., the nodes move with time in accordance with the moving boundary, a finite-difference mesh would be irregular and hence a finite-difference formulation would be very complicated. The finite-element approximation is based on the weak form of Eqs. (2.2) and (2.4).

Let $A(t)$ be the spatial region that the liquid occupies at time t, and D the space–time domain.

$$D = \{(x_i, t) : (x_i) \in A(t), t > 0\}.$$

Then the weak form of the conservation equations may be written as

$$\int_D \phi \left(\frac{\partial u_i}{\partial t} + \frac{\partial}{\partial x_j} \left(u_j u_i + p\delta_{ij} - \nu \frac{\partial u_i}{\partial x_j} \right) \right) dV = \int_D \phi f_i \, dV, \tag{2.6}$$

$$\int_{A(t)} \psi \frac{\partial u_j}{\partial x_j} \, dA = 0, \tag{2.7}$$

where the arbitrary functions ϕ and ψ are required to be measurable in the Sobolev sense and ϕ vanishes on that part of the boundary of $A(t)$ which satisfies the no-slip condition. Solutions u_i and p are required to have measurable derivatives of order 2 and 1, respectively.

From a computational viewpoint a more useful weak form is the Galerkin form which is derived from (2.6) by the use of Green's theorem. This form requires minimum continuity of the solutions u_i and p.

$$\int_D \phi \left(\frac{\partial u_i}{\partial t} - \frac{\partial \phi}{\partial x_j} \left(u_j u_i + p\delta_{ij} - \nu \frac{\partial u_i}{\partial x_j} \right) \right) dV$$

$$+ \int_{C(t)} \phi \left(u_j u_i + p\delta_{ij} - \nu \frac{\partial u_i}{\partial x_j} \right) n_j \, ds \, dt$$

$$= \int_D \phi f_i \, dV, \tag{2.8}$$

where the integration in s is over the free boundary of $A(t)$, and $C(t)$ is the domain

$$C(t) = \{(x_i, t): (x_i) \in \delta A_s(t), t > 0\},$$

where $\delta A_s(t)$ is the free boundary of $A(t)$. Here ϕ is required to have measurable first derivatives and a solution is sought such that u_i has measurable first derivatives and p is measurable. The natural boundary condition on the free surface is incorporated by the replacement of

$$\left(p\delta_{ij} - \nu \frac{\partial u_i}{\partial x_j} \right) n_j$$

by

$$\nu \frac{\partial u_j}{\partial x_i} n_j - \gamma \left(\frac{1}{R_1} + \frac{1}{R_2} \right) n_i, \tag{2.9}$$

from (2.3).

Equations (2.7) and (2.8) form the basis of the finite-element method to be considered in the next section.

III. Galerkin Approximation

At this stage it is assumed that the solution to the set of conservation equations is given at some time t^n and that the solution at some later time t^{n+1} is desired. For simplicity we restrict ourselves to plane flow and in particular to plane flow constrained to move within the region $0 \leqslant x \leqslant X$, $y \geqslant 0$ (see Fig. 1) although what follows can be easily generalised. Hence D^n is defined to be the region in space-time containing the fluid between the times t^n and t^{n+1} (see Fig. 2).

$$D^n = \{(x_i, t): (x_i) \in A(t), t^n \leqslant t \leqslant t^{n+1}\}.$$

Then (2.7) and (2.8) may be rewritten as

$$\int_{A(t^{n+1})} \psi \frac{\partial u_j}{\partial x_j} \, dA = 0, \tag{3.1}$$

$$\int_{D^n} \phi \frac{\partial u_i}{\partial t} - \frac{\partial \phi}{\partial x_j}\left(u_j u_i + p\delta_{ij} - \nu \frac{\partial u_i}{\partial x_j}\right) dV$$

$$+ \int_{C^n} \phi \left(u_j u_i + \nu \frac{\partial u_j}{\partial x_i} - \gamma \frac{1}{R}\delta_{ij}\right) n_j \, ds \, dt$$

$$= \int_{D^n} \phi f_i \, dV, \tag{3.2}$$

where

$$C^n = \{(x_i, t): (x_i) \in \delta A_s(t), t^n \leqslant t \leqslant t^{n+1}\}.$$

To approximate the problem (3.1) and (3.2) with the appropriate boundary and

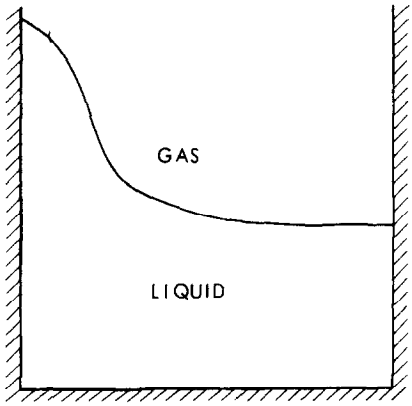

FIG. 1. Fluid-filled domain $A(t^n)$.

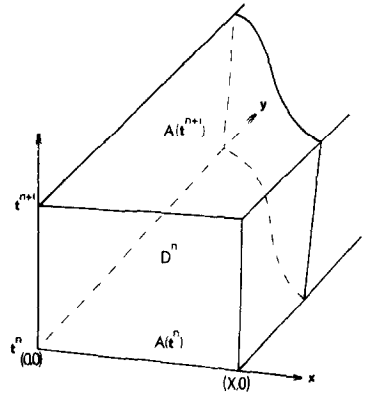

FIG. 2. The space-time domain D^n.

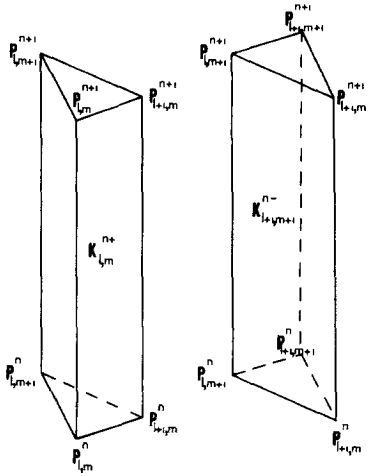

FIG. 3. Triangular prisms $K^{n+}_{l,m}$ and $K^{n-}_{l+1,m+1}$ used to approximate D^n.

initial conditions, we approximate the region D^n by a set of finite elements, in particular a set of triangular prisms designated by $K^{n+}_{l,m}$ and $K^{n-}_{l,m}$ (see Fig. 3) whose nodes are designated by $P^n_{l,m}$ for $0 \leqslant l \leqslant L$, $0 \leqslant m \leqslant M$. For flexibility both the x-coordinate and y-coordinate of each of the nodes may be varied at each time level in any appropriate manner which makes allowance for the changing shape of the fluid-filled region. For our purposes and because it simplifies the algebra, we choose to make the x-coordinate of each node independent of the y-coordinate. Hence the nodes $P^n_{l,m}$ will have coordinates of the form (see Fig. 4)

$$P^n_{l,m} = (x^n_l, y^n_{l,m}).$$

For some problems it may be desirable to have greater flexibility in the choice of the nodes of the elements and hence to allow the x-coordinate to be dependent on the y-

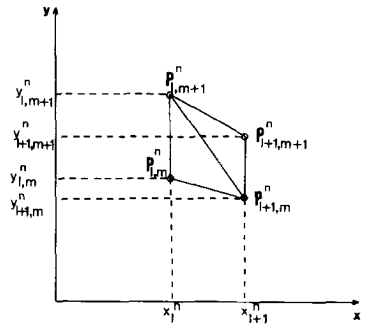

FIG. 4. The coordinates of the nodes $P^n_{l,m}$, $P^n_{l+1,m}$, $P^n_{l,m+1}$, and $P^n_{l+1,m+1}$ of the triangular bases of $K^{n+}_{l,m}$ and $K^{n-}_{l+1,m+1}$ at $t = t^n$.

coordinate. In such cases (3.4) below would be replaced by an equation of the form (3.5) with y replaced by x. Clearly the triangular bases of these prisms are an approximation to the regions $A(t^n)$ and $A(t^{n+1})$. Denote by $\delta K_{l,m}^{n+}$ the triangular base of $K_{l,m}^{n+}$ at the time t^{n+1}. Equations (3.1) and (3.2) may now be approximated by the sum of integrals over $K_{l,m}^{n+}$ and $K_{l,m}^{n-}$ and their bases. For free boundary problems these elements will change in shape and so to facilitate the evaluation of integrals over these elements, parametric transformations are introduced which map them onto the standard prism K^+ (see Fig. 5).

From geometrical considerations we construct the parametric transformation $(t, x, y) \to (\xi, \beta, \eta)$ from $K_{l,m}^{n+}$ to K^+ in the form

$$t = (1 - \xi)\, t^n + \xi t^{n+1}, \tag{3.3}$$

$$x = (1 - \beta)\, x_l^{n+\xi} + \beta x_{l+1}^{n+\xi}, \tag{3.4}$$

$$y = (1 - \beta - \eta) y_{l,m}^{n+\xi} + \beta y_{l+1,m}^{n+\xi} + \eta y_{l,m+1}^{n+\xi}; \qquad 0 \leqslant \xi, \quad \beta \leqslant 1, \quad \eta \leqslant 1 - \beta, \tag{3.5}$$

where the following convention has been used

$$y_{l,m}^{n+\xi} = (1 - \xi)\, y_{l,m}^n + \xi y_{l,m}^{n+1}.$$

Similar transformations exist for $K_{l,m}^{n-}$ onto K^+ with the nodes $P_{l+1,m}^n$ and $P_{l,m+1}^n$ replaced by the nodes $P_{l-1,m}^n$ and $P_{l,m-1}^n$ in the above equations.

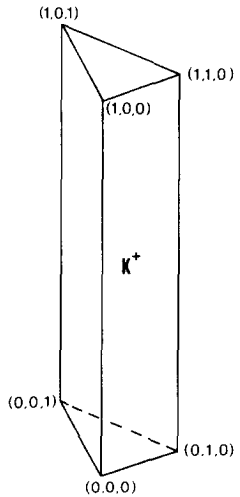

FIG. 5. Standard prism K^+.

The inverse transformations are

$$\xi = \frac{t - t^n}{t^{n+1} - t^n}, \tag{3.6}$$

$$\beta = \frac{x - x_l^{n+\xi}}{x_{l+1}^{n+\xi} - x_l^{n+\xi}}, \tag{3.7}$$

$$\eta = \frac{y - \beta y_{l+1,m}^{n+\xi} - (1-\beta)\, y_{l,m}^{n+\xi}}{y_{l,m+1}^{n+\xi} - y_{l,m}^{n+\xi}}. \tag{3.8}$$

The coordinates (ξ, β, η) of the nodes of K^+ are as shown in Fig. 5.

The subdivision of the domain D^n into a set of finite elements reduces the original problem to one which is finite dimensional and for which the values of velocity and pressure are required only at the nodes of the element. In terms of the nodal values, the Galerkin approximation for the solution of (3.1) and (3.2) is taken to be of the form

$$u_i \approx \hat{u}_i = \sum_{l=1}^{L-1} \sum_{m=1}^{M} \phi^{l,m}(x, y)\, u_{l,m}^{(i)}(t) + v_i, \tag{3.9}$$

$$p \approx \hat{p} = \sum_{l=1}^{L} \sum_{m=1}^{M} \psi^{l,m}(x, y)\, p_{l,m}(t), \tag{3.10}$$

where

$$u_{l,m}^{(i)}(t) = (1 - \xi)\, u_{l,m}^{(i)n} + \xi u_{l,m}^{(i)n+1}, \tag{3.11}$$

$$\begin{aligned} p_{l,m}(t) &= (1 - \xi)\, p_{l,m}^n + \xi p_{l,m}^{n+1} \\ &= p_{l,m}^{n+\xi} \end{aligned} \tag{3.12}$$

and $u_{l,m}^{(i)n}$, $p_{l,m}^n$ are the nodal values of $\hat{u}_i$ and $\hat{p}$ at time t^n; $\phi^{l,m}$ and $\psi^{l,m}$ are interpolating functions and are assumed to form a complete set of functions over the fluid-filled space; and v_i are functions satisfying the no-slip boundary conditions and are zero elsewhere. The Galerkin approximation satisfies

$$\int_{A(t^{n+1})} \psi^{l,m} \frac{\partial \hat{u}_j}{\partial x_j}\, dA = 0, \tag{3.13}$$

$$\begin{aligned} &\int_{D^n} \left(\phi^{l,m} \frac{\partial \hat{u}_i}{\partial t} - \frac{\partial \phi^{l,m}}{\partial x_j} \left(\hat{u}_j \hat{u}_i + \hat{p}\delta_{ij} - \nu \frac{\partial \hat{u}_i}{\partial x_j} \right) \right) dV \\ &\quad + \int_{C^n} \phi^{l,m} \left(\hat{u}_j \hat{u}_i + \nu \frac{\partial \hat{u}_j}{\partial x_i} - \gamma \frac{1}{R} \delta_{ij} \right) n_j\, ds\, dt \\ &\quad = \int_{D^n} \phi^{l,m} f_i\, dV. \end{aligned} \tag{3.14}$$

The interpolating functions $\phi^{l,m}$ must be chosen to preserve continuity of velocity between the elements. This is the minimum continuity requirement on the velocity and is necessary because of first-order derivatives in Eq. (3.2). No such continuity requirement is necessary for the interpolating functions $\psi^{l,m}$. In particular, $\phi^{l,m}$ are chosen to be the set of pyramid functions which within each element are linear in η and β

$$\phi^{l,m}(P^n_{a,b}) = \delta^{lm}_{ab} = \begin{cases} 1, & l=a, \quad m=b \\ 0 & \text{otherwise.} \end{cases} \tag{3.15}$$

The $\psi^{l,m}$ are chosen to be the set of step functions:

$$\psi^{l,m} = \begin{cases} 1, & (x,y) \in \delta K^{n+}_{l-1,m-1} \quad \text{or} \quad \delta K^{n-}_{l,m} \\ 0 & \text{otherwise.} \end{cases} \tag{3.16}$$

The exact form of $\phi^{l,m}$ and $\psi^{l,m}$ can be better seen by considering the approximation for u_i, p in the elements $K^{n+}_{l,m}$ and $K^{n-}_{l,m}$. Thus in $K^{n+}_{l,m}$

$$u_i = (1-\beta-\eta)\, u^{n+\xi}_{l,m} + \beta u^{n+\xi}_{l+1,m} + \eta u^{n+\xi}_{l,m+1}, \tag{3.17}$$

$$p = p^{n+\xi}_{l+1,m+1}, \tag{3.18}$$

$$\phi^{l,m} = (1-\beta-\eta), \tag{3.19a}$$

$$\phi^{l+1,m} = \beta, \tag{3.19b}$$

$$\phi^{l,m+1} = \eta, \tag{3.19c}$$

$$\psi^{l+1,m+1} = 1. \tag{3.20}$$

Similar approximations exist in $K^{n-}_{l,m}$ with nodes $P^n_{l+1,m}$ and $P^n_{l,m+1}$ replaced by $P^n_{l-1,m}$ and $P^n_{l,m-1}$, respectively, in (3.17) and with $p^{n+\xi}_{l+1,m+1}$ replaced by $p^{n+\xi}_{l,m}$ in (3.18).

Equations (3.13) and (3.14) provide a system of equations for which we can solve for $u^{(l)^n}_{l,m}$ and $p^n_{l,m}$ subject to the initial and boundary conditions. We need one more equation to determine the position of the free surface. This is furnished by the equation

$$\frac{\partial y_h}{\partial t} + u\frac{\partial y_h}{\partial x} = v, \tag{3.21}$$

where y_h is the height of the free surface above the x-axis, u is the velocity on the surface in the x direction, and v is the velocity in the y direction. Again we choose to work with the integrated weak form of this equation.

$$\int_{t^n}^{t^{n+1}} \int_0^X \left(\phi_1 \frac{\partial y_h}{\partial t} - \phi_1 y_h \frac{\partial u}{\partial x} - u y_h \frac{\partial \phi_1}{\partial x} \right) dx\, dt = \int_{t^n}^{t^{n+1}} \int_0^X \phi_1 v\, dx\, dt. \tag{3.22}$$

The Galerkin approximation for y_h is then given by

$$y_h \approx \hat{y}_h = \sum_{l=0}^{L} \phi_1^l(x)\, y_{l,M}(t),$$

where

$$y_{l,M}(t) = y_{l,M}^{n+\xi},$$

and

$$\phi_1^l(x) = \delta_a^l = \begin{cases} 1, & l = a \\ 0 & \text{otherwise.} \end{cases}$$

The reciprocal of the radius of curvature, given by

$$\frac{1}{R} = \frac{d^2 y_h/dx^2}{(1 + [dy_h/dx]^2)^{3/2}}, \tag{3.23}$$

is approximated at each surface node $P_{l,M}^n$ using the following finite difference approximations for derivatives of y_h at each node.

$$\frac{dy_h}{dx} \simeq \frac{1}{(\Delta x_l^n + \Delta x_{l-1}^n)} \cdot \left(\frac{\Delta x_l^n}{\Delta x_{l-1}^n} \cdot (y_{l,M}^n - y_{l-1,M}^n) + \frac{\Delta x_{l-1}^n}{\Delta x_l^n} \cdot (y_{l+1,M}^n - y_{l,M}^n) \right), \tag{3.24}$$

$$\frac{d^2 y_h}{dx} \simeq \frac{2}{(\Delta x_l^n + \Delta x_{l-1}^n)} \cdot \left(\frac{(y_{l+1,M}^n - y_{l,M}^n)}{\Delta x_l^n} - \frac{(y_{l,M}^n - y_{l-1,M}^n)}{\Delta x_{l-1}^n} \right), \tag{3.25}$$

where

$$\Delta x_l^n = x_{l+1}^n - x_l^n, \qquad l = 0, L. \tag{3.26}$$

IV. Numerical Quadrature and Computational Techniques

In this section we consider the quadrature formulas used to evaluate the integrals that occur in (3.13), (3.14), and (3.22) and the computational techniques involved in solving the resulting system of finite-difference equations.

Integrals over $K_{l,m}^{n+}$ and $K_{l,m}^{n-}$ are converted by the parametric transformation introduced in Section III into integrals over the standard element K^+.

$$\iiint_{K_{l,m}^{n+}} \Psi \, dV = \iiint_{K^+} \Psi J_{l,m}^{n+} \, d\eta \, d\beta \, d\xi, \tag{4.1}$$

where Ψ is some arbitrary function, $\hat{\Psi}$ the Galerkin approximation for Ψ, and $J_{l,m}^{n+}$ is the Jacobian of the transformation

$$J_{l,m}^{n+} = (t^{n+1} - t^n)(x_{l+1}^{n+\xi} - x_l^{n+\xi})(y_{l,m+1}^{n+\xi} - y_{l,m}^{n+\xi}).$$

Rather than evaluate the integral on the right side of (4.1) as it stands we use the following quadrature formula for integrals over K^+

$$\iiint_{K^+} \Phi \, d\eta \, d\beta \, d\xi = \tfrac{1}{12} [\Phi(0,0,0) + \Phi(1,0,0) + \Phi(0,1,0) + \Phi(1,1,0) + \Phi(0,0,1) + \Phi(1,0,1)], \tag{4.2}$$

where $\Phi(0,0,0)$ is the nodal value of the integrand at node $(0,0,0)$ of the element K^+. Similar simple quadrature formulas are used to evaluate integrals over $\delta K_{l,m}^{n+}$, $\delta K_{l,m}^{n-}$ and over boundaries of D^n.

For Eq. (3.14) with test function $\phi^{l,m}$ integrals over D^n reduce to the sum of integrals over the neighbouring elements with the node $P_{l,m}^{n+1}$ in common (see Fig. 6). Similarly for Eq. (3.13) with test function $\psi^{l,m}$ integrals over $A(t^{n+1})$ reduce to the sum of integrals over $\delta K_{l,m}^{n+}$ and $\delta K_{l+1,m+1}^{n-}$ (see Fig. 7). Equation (3.14) is non-linear, so some iterative procedure is in general necessary for the solution of the system of equations generated by the above quadrature formulas. However for the low Reynold's number flow problems, to be considered here, the equations may be linearised by approximating the inertia terms at t^{n+1} by their values at t^n. Then if we choose as our solution vector

$$\mathbf{X}^{n+1} = (\mathbf{X}_l^{n+1}), \qquad l = 1, \quad L-1,$$

where

$$\mathbf{X}_l^{n+1} = \begin{pmatrix} u_{l,m}^{n+1} \\ p_{l,m}^{n+1} \\ v_{l,m}^{n+1} \end{pmatrix}, \quad m = 1, M,$$

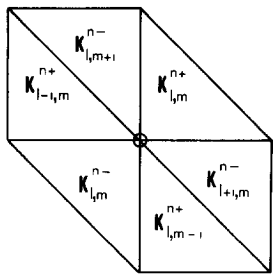

FIG. 6. The elements that have the node $P_{l,m}^{n+1}$ as a common node.

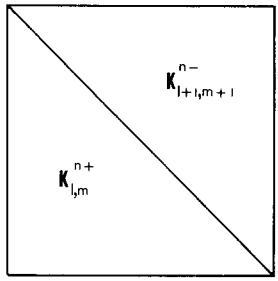

FIG. 7. Elements for which $\psi^{l,m}$ is non-zero.

the system of equations takes the form

$$\mathsf{M}\mathbf{X}^{n+1} = \mathbf{b}^n, \tag{4.3}$$

where M is a block-tridigonal matrix and **b** contains the forcing terms and information about the flow at time t^n. Although this choice of arrangement of the equations does not yield a symmetric matrix, it has the advantage that the diagonal blocks in M are only of order $3M \times 3M$ so that, if a standard block elimination technique with Gaussian elimination is used, there is only of the order of $\frac{5}{3}(L-1)M^3$ operations necessary to solve for $\mathbf{X}^{n+1}$.

Clearly the choice of the elements K_m^{n+} and K_m^{n-} is dependent on the position of the free surface which in turn is dependent on the values of the velocity on the free surface at time t^{n+1}. Hence an iterative procedure is necessary. The system of equations derived from (3.2) takes the form

$$\mathsf{N}(\mathbf{X}^{n+1})\,\mathbf{y}^{n+1} = \mathbf{c}^n, \tag{4.4}$$

where N is a tridiagonal matrix which depends on the solution vector $\mathbf{X}^{n+1}$, $\mathbf{y}^{n+1}$ is the vector $(y_{l,M}^{n+1})$, and **c** contains terms determined at t^n. Equations (4.3) and (4.4) are solved iteratively in the following manner,

$$\begin{aligned} \mathsf{N}(\mathbf{X}^{n+1(v)})\,\mathbf{y}^{n+1(v+1)} &= \mathbf{c}^n, \\ \mathsf{M}(y^{n+1(v+1)})\,\mathbf{X}^{n+1(v+1)} &= \boldsymbol{b}^n, \qquad v = 0, 1, \ldots, \end{aligned} \tag{4.5}$$

where

$$\mathbf{X}^{n+1(0)} = \mathbf{X}^n.$$

For the problems we considered it was found that this iterative scheme gave convergence to five significant figures in two or three iterates.

V. Numerical Results

In this section we present results for the entrainment and the circulation problems. The cases presented are those that gave the greatest displacement of the free surface from its original configuration and hence best illustrate the power of this method.

Both of the problems were impulsively started and hence displayed Rayleigh boundary layer effects. The propagation of this boundary layer restricted the size of the initial time steps in as much as it was not possible to choose an initial time step which was so large that the Rayleigh layer could propagate through the entire fluid region. However, once initiated, there was essentially no restriction on the size of the time step used due to the implicit nature of the time-stepping algorithm.

In the entrainment problem, we consider the flow generated by the withdrawal of a vertical plate from a fluid bath (see Fig. 8). Initially the fluid is stationary and occupies the region $0 < x < L$, $0 < y < d$. The top surface is free. The boundaries $x = L$ and $y = 0$ are stationary and the boundary $x = 0$ moves upward with a speed U. We used as non-dimensional variables,

$$u' = u\left(\frac{d}{LU}\right),$$

$$v' = \frac{v}{U},$$

$$p' = \frac{p}{gd},$$

$$x' = \frac{x}{L},$$

$$y' = \frac{y}{d},$$

$$t' = \left(\frac{v}{d^2}\right)t,$$

where g is the gravitational constant.

The three non-dimensional parameters that arise due to this scaling are the Reynold's number,

$$\mathrm{Re} = \frac{Ud}{v},$$

the Froude number,

$$\mathrm{Fr} = \frac{U^2}{gd},$$

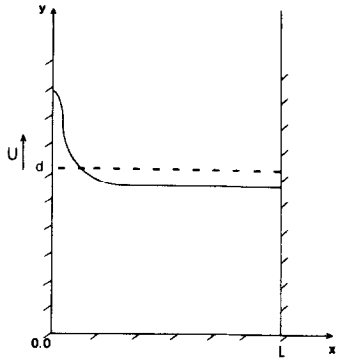

FIG. 8. Entrainment problem.

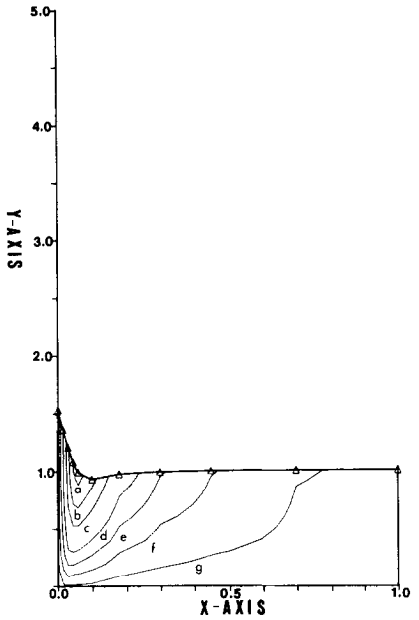

FIG. 9. Plot of the free surface for the entrainment problem with $\mathrm{Re} = 0.1$, $\gamma = 0$, $\mathrm{Fr} = 2.0$, $n = 0.1$, $t = 5.5$, $\Delta t = 1.0$, with stream lines (a)–(g) corresponding to -0.02, -0.016, -0.01, -0.006, -0.003, -0.001, -0.0001, respectively.

and the capillary number,

$$\mathrm{Ca} = \frac{vU}{\gamma}.$$

The theoretical treatments of this problem by Spiers *et al.* [10] and Gutfinger *et al.* [11] have been based on a one-dimensional boundary layer approximation of the flow

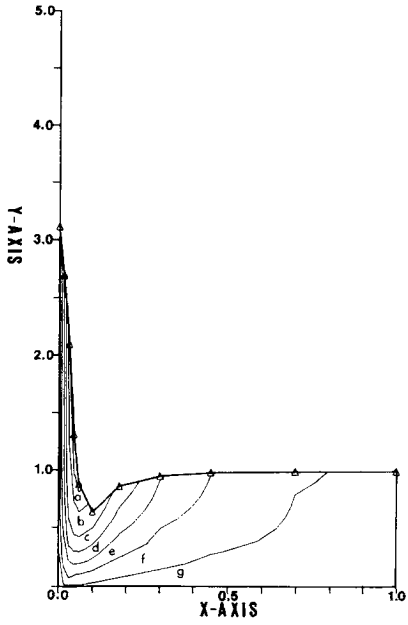

FIG. 10. Plot of free surface for $t = 20.5$.

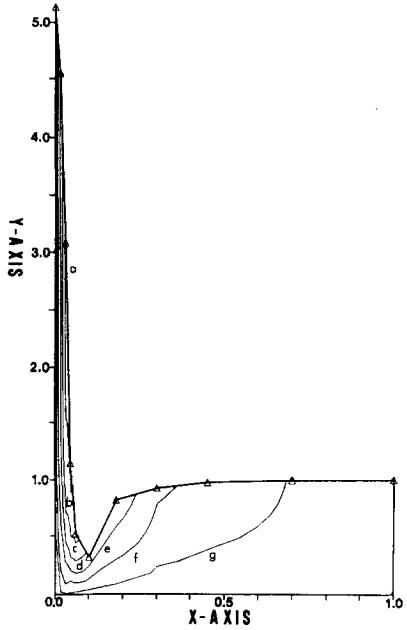

FIG. 11. Plot of free surface for $t = 38.5$.

equations in the region of the adhering film and also the existence of a "static meniscus" region to describe the shape of the film near the bath surface. Their theoretical results show good agreement with their experimental results for low values of the capillary number Ca. However, as they themselves acknowledge, the above assumptions are invalid for large values of Ca, and there exists a discrepancy between their theoretical and experimental results for Ca > 2. We have therefore considered two cases for this problem with values of Ca less than two and much greater than two, respectively.

The results presented in Figs. 9–11 are for the case Re = 0.1, Fr = 2.0, $\gamma = 0$ and aspect ratio $n = 0.1$ ($n = d/L$). These diagrams show the development of a film of liquid on the vertically moving wall and illustrate the laminar nature of the flow in this region. They also show that the effects of the entrainment is localized in a region immediately adjacent to the moving wall and show the absence of any circulation of the flow within the bath itself. The region of constant film thickness also appears to form very close to the bath surface ($y \approx 1.2$) and its thickness is of the order of 0.05.

The results for the second case with Ca = 1.0, Re = 1.0, Fr = 0.01, and $n = 1.0$ are depicted in Figs. 12–14. Initially the presence of surface tension appears to create circulation effects in the region of the bath near the moving wall (Fig. 12). This effect then dissipates with the formation of a cell of circulation in the far corner of the bath away from the moving wall. Again a region of constant film thickness is beginning to

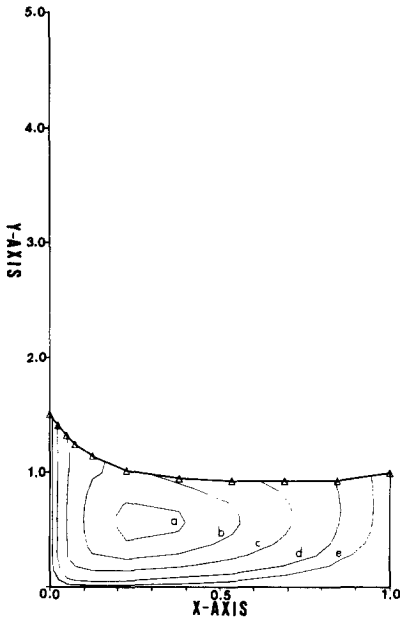

FIG. 12. Plot of the free surface for the entrainment problem with Re = 1.0, Fr = 0.01, $n = 1.0$, Ca = 1.0, $t = 0.51$, $\Delta t = 0.01 - 0.1$, with streamlines (a)–(e) corresponding to −0.09, −0.06, −0.03, −0.009, −0.003, respectively.

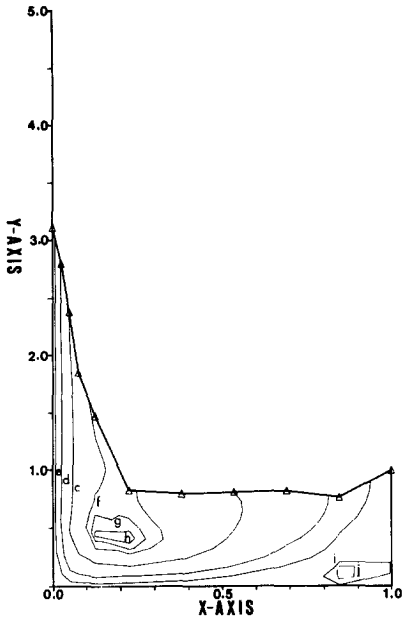

FIG. 13. Plot of free surface at $t = 2.21$ with streamlines (c), (d), and (e) as in Fig. 12 and with additional streamlines (f)–(j) corresponding to −0.05, −0.055, −0.058, +0.00005, +0.00001, respectively.

form on the moving wall, although this time at a greater distance from the surface of the bath ($y \approx 2.5$). The thickness of the film is of the order of 0.08 (see Fig. 14). These results are in marked contrast with those for zero surface tension effects.

As a measure of the accuracy of this method of solution we compared our results with those predicted by Spiers *et al.* [10] for an infinite sheet of entrained fluid with $\mathrm{Ca} = 1.0$. The dimensionless thickness h_0 of such a sheet can be determined using their theoretical and experimental results. It can be shown to be

$$h_0 = n \left(\frac{\mathrm{Fr}}{\mathrm{Re}}\right)^{1/2} T_0(\mathrm{Ca}), \tag{5.1}$$

where T_0 is a parameter dependent on Ca and can be determined from the experimental results to be equal to 0.75. Hence the estimated value of h_0 is 0.075. This is consistent with the results presented in Figs. 12–14.

For both cases the method proved to be highly stable even when the aspect ratios of the elements became extremely large (see Figs. 15–17), in fact the only limiting factor was the introduction of inaccuracies into the solution due to the relatively few number of elements (200) used and the simple interpolation formulas employed. These problems could be easily overcome by the introduction of a less sparse covering of the space-time domain. In addition the iterative procedure employed in

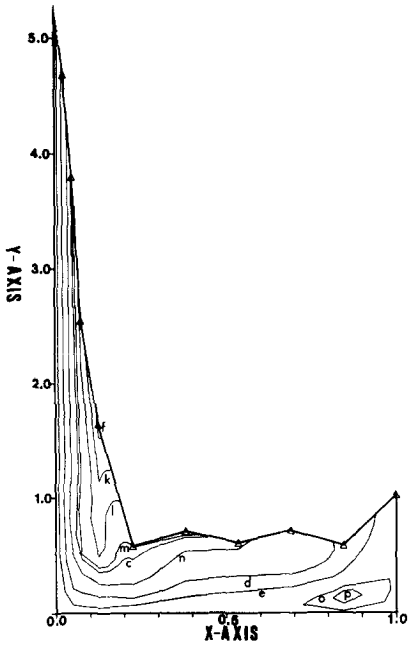

FIG. 14. Plot of free surface at $t = 4.31$ with streamlines (c), (d), (e) and (f) as in Fig. 13 and with additional streamlines (k)–(p) corresponding to −0.045, −0.04, −0.033, −0.02, +0.0001, +0.0006, respectively.

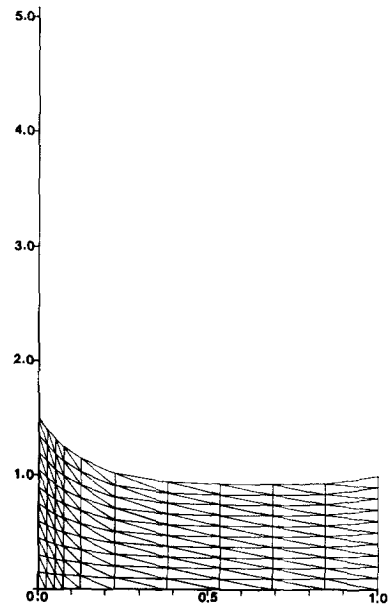

FIG. 15. Finite element mesh for the entrainment problem with $\mathrm{Re} = 1.0$, $\mathrm{Fr} = 0.01$, $n = 1.0$, $\mathrm{Ca} = 1.0$, and $t = 0.51$.

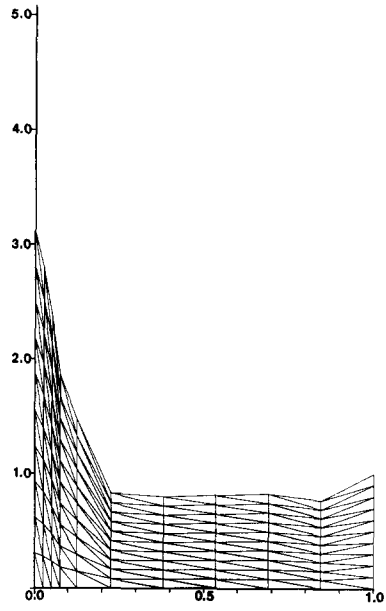

FIG. 16. Finite-element mesh at $t = 2.21$.

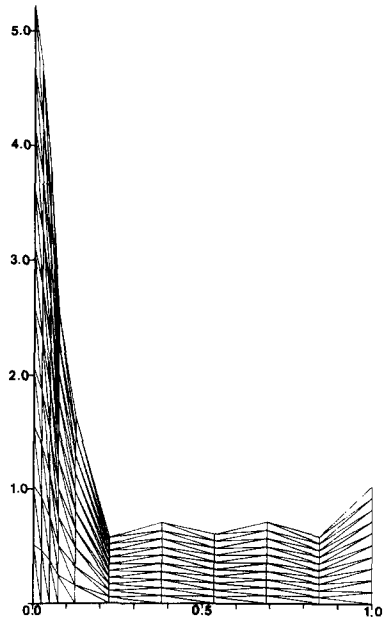

FIG. 17. Finite-element mesh at $t = 4.31$.

this method gave excellent convergence to five decimal places within two or three iterates for time steps varying from 0.01 to 1.0.

In the circulation problem, we consider the flow generated in the bath by the motion of the horizontal wall $y = 0$ (see Fig. 18). Initially the fluid is stationary and occupies the region $0 < x < L$, $0 < y < d$. The top surface is free and the boundaries $x = 0$ and $x = L$ are stationary and the boundary $y = 0$ moves horizontally with a speed U.

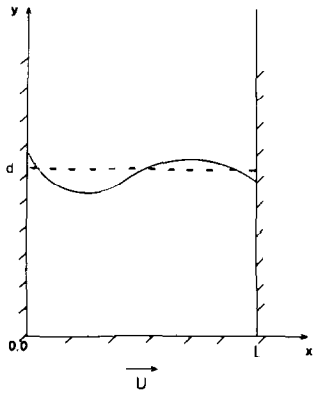

FIG. 18. Channel circulation problem.

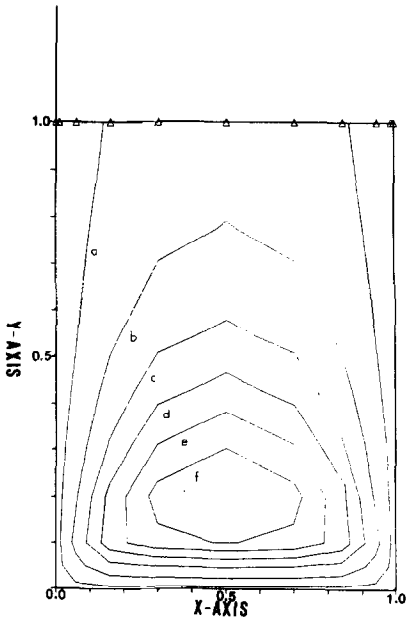

FIG. 19. Plot of free surface for the circulation problem with Re = 1.0, Fr = 10^4, $n = 1.0$, $t = 0.01$, and $\Delta t = 0.01 - 0.1$ with streamlines (a)–(f) corresponding to 0.001, 0.005, 0.01, 0.015, 0.02, 0.025, respectively.

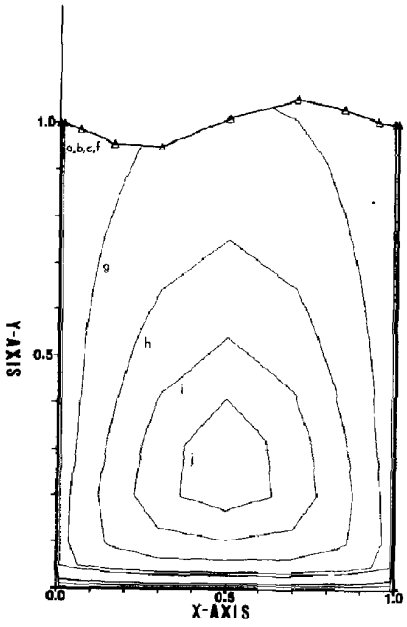

FIG. 20. Plot of free surface at $t = 1.75$ with streamlines (a)–(f) as in Fig. 19 and with additional streamlines (g)–(j) corresponding to 0.03, 0.05, 0.075, 0.095, respectively.

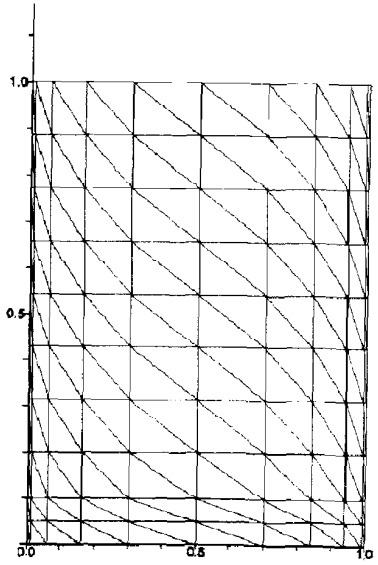

FIG. 21. Finite-element mesh for the circulation problem at $t = 0.01$.

We used as non-dimensional variables,

$$u' = \frac{u}{U},$$

$$v' = \left(\frac{L}{dU}\right) v,$$

$$x' = \frac{x}{L},$$

$$y' = \frac{y}{d},$$

$$p' = \frac{p}{gd},$$

$$t' = \left(\frac{v}{d^2}\right) t.$$

The results are presented graphically in Figs. 19 and 20 for the case $\mathrm{Re} = 1.0$, $\mathrm{Fr} = 10^4$, $\gamma = 0$ and aspect ratio $n = 1.0$. Our results indicate that a steady-state solution exists for this problem.

As a test of the general nature of our solution we can compare our results with those of Pan and Acrivos [12] and Torrance *et al.* [13] for the cavity-driven problem. Although there are important differences between the present free surface problem

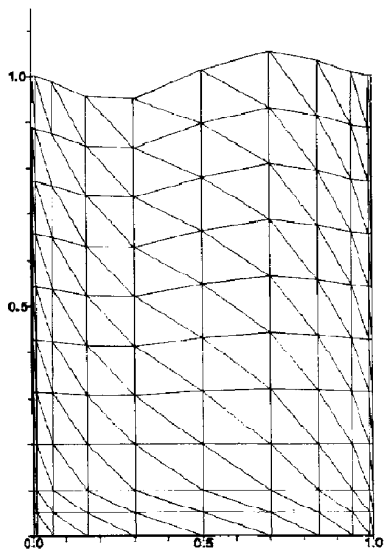

FIG. 22. Finite-element mesh at $t = 1.75$.

and the cavity-driven problem, they are similar in the sense that away from the free surface the streamlines have a similar nature.

Figure 19 gives a plot of the stream function immediately after the liquid is set in motion. Subsequently, as the Rayleigh layer propagates through the liquid, the free surface is progressively distorted until a standing wave form is set up as illustrated in Fig. 20. The solution at this stage was unchanging in the third decimal place and appears to have reached a steady state. Figures 21 and 22 show the initial and final mesh configuration, respectively.

Again convergence was excellent with five decimal agreement after two or three iterates ($\Delta t = 0.01 - 0.1$) and again, except for the initial stages, there was no effective restriction on the size of the time step.

VI. Conclusion

Because of the highly stable and convergent nature of this method, even for very large time steps, the authors feel that it will prove a useful and powerful tool in the solution not only of free boundary flow, but generally of time-dependent fluid dynamical problems. The authors are at present looking at the adaptation of this method to more difficult problems, such as those involving three dimensions.

Acknowledgment

One of us (C.S.F.) would like to acknowledge the financial help given by a Commonwealth Postgraduate Research Award during the completion of this work.

References

1. F. H. Harlow and J. E. Welch, *Phys. Fluids* **8** (1965).
2. C. W. Hirt, J. L. Cook, and T. D. Butler, *J. Comput. Phys.* **5** (1970), 103–124.
3. B. D. Nichols and C. W. Hirt, *J. Comput. Phys.* **8** (1971), 434–448.
4. C. W. Hirt, A. A. Amsden, and J. L. Cook, *J. Comput. Phys.* **14** (1974), 227–253.
5. R. E. Nickell, R. I. Tanner, and B. Caswell, *J. Fluid. Mech.* **65** (1974), 189–206.
6. E. G. Thompson, L. R. Mack, and F. S. Lin, *in* "Developments in Mechanics," Vol. 5, Proceedings of the 11th Midwestern Mechanics Conference.
7. R. Bonnerot and P. Jamet, *Int. J. Num. Meth. Eng.* **8** (1974), 811–820.
8. P. Jamet and R. Bonnerot, *J. Comput. Phys.* **18** (1975), 297–308.
9. R. Bonnerot and P. Jamet, *J. Comput. Phys.* **25** (1977), 163–181.
10. R. P. Spiers, C. V. Subbaraman, and W. L. Wilkinson, *Chem. Eng. Sci.* **29** (1974), 389–396.
11. C. Gutfinger and J. A. Tallmadge, *A. I. Ch. E. J.* **11** (1965).
12. F. Pan and A. Acrivos, *J. Fluid Mech.* **28** (1967), Part 4, 643–655.
13. K. Torrance, R. Davis, K. Eike, P. Gill, D. Gutman, A. Hsui, S. Lyons, and H. Zien, *J. Fluid Mech.* **51** (1972), Part 2, 221–231.
14. J. T. Oden, *Int. J. Num. Math. Engrg.* 1(1969), Part I, 247–259; Part II, 205–221.